Rigid-Rod-Like Main Chain Polymers with Rigidly Attached Chromophores: A Novel Structural Concept for Electrooptical Materials. 2. Theory and Electrooptical Measurements

C. Heldmann,† D. Neher,* H.-J. Winkelhahn, and G. Wegner

MPI für Polymerforschung, Ackermannweg 10, D-55128 Mainz, FRG

Received March 5, 1996[⊗]

ABSTRACT: A theoretical approach to describe the electrooptical properties of rigid-like polymers with NLO-active chromophores rigidly attached to the main chains is developed and the results are compared with the experimental data. Due to the particular structure of the polymer, the motion of the chromophores is restricted to the two dimensional rotation of the chromophore around the main chain. Theoretical computations based on Boltzmann-weighted distribution functions predict a pronounced effect of this dimensional restriction on the nonlinear optical properties. In particular, the relaxation of the polar order induced by a strong electrical poling field is shown to be significantly slowed down in comparison to conventional flexible and three-dimensionally mobile main chain systems. Structural investigations on spin-cast films of the polymers designed to realize this concept show a layered morphology with the polymer main chains oriented parallel to the substrate plane. Due to the anisotropic structure, the ratio of the nonzero tensor components $\chi^{(2)}_{zzz}$ and $\chi^{(2)}_{xxx}$, as determined by attenuated total reflection, is well above three, in agreement with the theoretical predictions. The relaxation of the polar order is described by a multiexponential decay. The decay follows an Arrhenius-type time−temperature superposition law, which reflects a relaxation mechanism typical for locally activated processes.

Introduction

Recently, we synthesized a novel class of rigid rod polymers with NLO-active chromophores, where some of the side chains are replaced by nonlinear optically active chromophores which are attached normal the main chain axis (Figure 1b in ref 1). As thoroughly discussed below, this particular arrangement will induce three distinct features:

(i) Most polymer based systems have in common that the chromophores possess rotational freedom in three dimensions. In the proposed concept the rotational motion is restricted to only two dimensions (namely, the rotation of the chromophore around the stiff main chain axis).

(ii) Providing a parallel orientation of the polymer main chains with respect to the film surface, the ratio of the non-zero tensor components will be highly sensitive to the bonding angle between the chromophore axis and the backbone direction. In particular, the layered architecture is expected to support an upright orientation of the chromophore with respect to the main chain as shown in Figure 1b in ref 1.

(iii) It is an important feature of this concept that the chromophores are rigidly attached to the main chains. Therefore, the relaxation of the induced polar order will only depend on the dynamics of the main chains and will be almost decoupled from the dynamics of the (solubility-mediating) flexible side chains in the microphase-separated layered structure. Thus, we expected a drastically improved long term stability of the polar order even at higher temperatures (> 100 °C).

In the first part of the paper we will provide the theoretical background for the description of the nonlinear optical properties and the dynamical behavior of these particular compounds in comparison with conventional three-dimensional systems (e.g., polymers with flexible main chains). The physical properties will be discussed in detail in the second part.

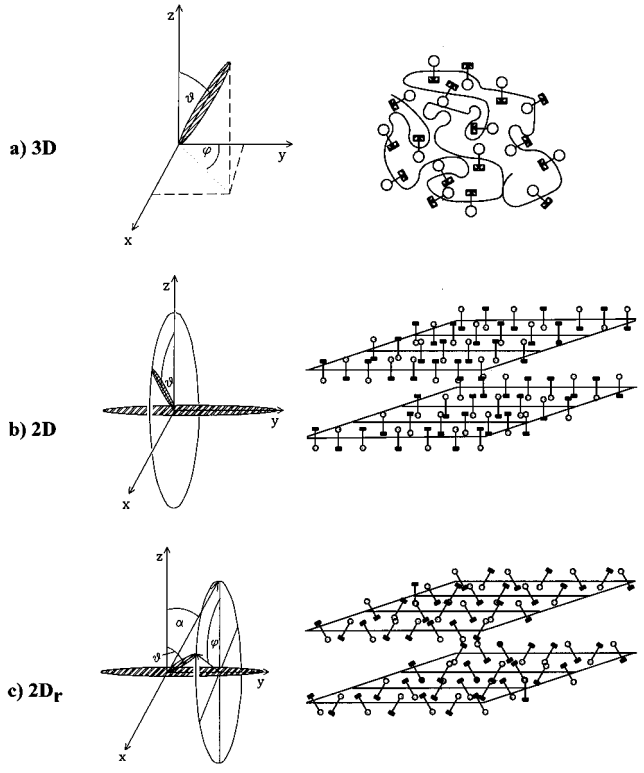

Figure 1. Illustration of the three different geometries discussed in the text: (a) the chromophore is bonded to a flexible main chain resulting in an isotropic three dimensional orientational distribution $F_{3D}(\vartheta)$, (b) the chromophore is bonded to a rigid rod main chain with the chromophore axis normal to the direction of the polymer chain, resulting in a two dimensional distribution $F_{2D}(\vartheta)$, (c) the chromophore is again rigidly attached to the rigid backbone but with an angle $a \neq 0$ relative to the normal of the polymer chain. This leads to an angular restricted distribution $F_{2Dr}(\vartheta)$.

* To whom correspondence should be addressed.
† Current address: Cavendish Laboratory, Madingley Road, Cambridge CB3 OHE, England.
⊗ Abstract published in *Advance ACS Abstracts,* May 1, 1996.

S0024-9297(96)00353-1 CCC: $12.00

Theory

In the following we compare three different geometries shown in Figure 1. In case (a), the chromophore is linked to a flexible main chain with rotational freedom in all directions. In case (b), the chromophore is perpendicularly attached to a rigid rod backbone. The main chains lie in the $x-y$ plane with no preferential orientation within the plane. In case (c), the chromophore is attached to a rigid rod main chain with an angle $\alpha \neq 0$ with respect to the z-axis. In all cases the poling field E_{pol} is applied parallel to z. Due to the orientational symmetry within the substrate plane, there are only two independent components of the nonlinear optical susceptibility tensor $\chi^{(2)}$:[2]

$$\chi^{(2)}_{ZZZ}(-\omega_3; \omega_2, \omega_1) = N f_{\omega 1} f_{\omega 2} f_{\omega 3} \beta_{zzz}(-\omega_3; \omega_2, \omega_1) \int_\vartheta \cos^3 \vartheta \, F(\vartheta) \, d\vartheta$$

$$\chi^{(2)}_{XXZ}(-\omega_3; \omega_2, \omega_1) = {}^1/_2 N f_{\omega 1} f_{\omega 2} f_{\omega 3} \beta_{zzz}(-\omega_3; \omega_2, \omega_1) \int_\vartheta \sin^2 \vartheta \cos \vartheta \, F(\vartheta) \, d\vartheta \quad (1)$$

N is the chromophore number density, β_{zzz} the molecular hyperpolarizability of the chromophore along the main axis, $f_{\omega i}$ are the local field factors at frequencies ω_i, and $F(\vartheta)$ is the complete orientational distribution function that has to be determined separately for all three cases. The orientational distribution function under the influence of the external poling field E_{pol} can be computed from the orientational function $F(\vartheta, E=0)$ without poling field multiplied by the Boltzmann factor.

$$F(\vartheta, E_{pol}) = F(\vartheta, 0) \exp(m \cos \vartheta) \quad (2)$$

with

$$m = \frac{\mu_g E_{pol} f_o}{k T_{pol}} \quad (3)$$

μ_g is the dipole moment of the chromophore in the ground state, k the Boltzmann constant, T_{pol} the poling temperature, and f_o an Onsager type local field factor.[2]

For case (a), with the chromophores isotropically distributed in three dimensions, $F(0) = F_{3D}(0)$ is given by the differential solid angle factor $\sin \vartheta$, resulting in

$$\int_0^\pi F_{3D}(\vartheta, E) \, d\vartheta = K' \int_0^\pi \sin \vartheta \, e^{m \cos} \, d\vartheta \quad (4)$$

K', K'' (eq 5), and K''' (eq 8) are normalization factors. The function F_{2D} for case (b) can be derived through the Boltzmann-weighted rotation around the rigid rod backbone:

$$\int_0^\pi F_{2D}(\vartheta) \, d\vartheta = K'' \int_0^\pi e^{(\mu E \cos \vartheta)/(kT)} \, d\vartheta \quad (5)$$

Note that in the 2D case the factor $\sin \vartheta$ is absent.

The 2D-restricted ($2D_r$) case (c) further includes the tilt angle α as defined in Figure 1. With φ describing the rotation of the chromophore around the main chain axis, the orientational distribution function $F_{2D,r}$ can be derived from the following equations:

$$\cos \vartheta = \frac{\vec{e}_Z \cdot \vec{e}_\mu}{e_Z e_\mu} = \cos \alpha \cos \varphi \quad (6)$$

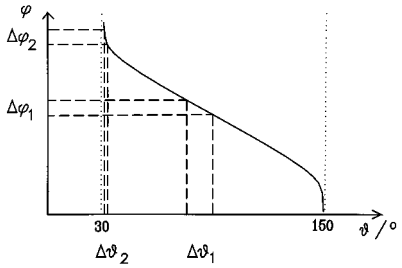

Figure 2. Illustration of eq 6 leading to the derivative in eq 7.

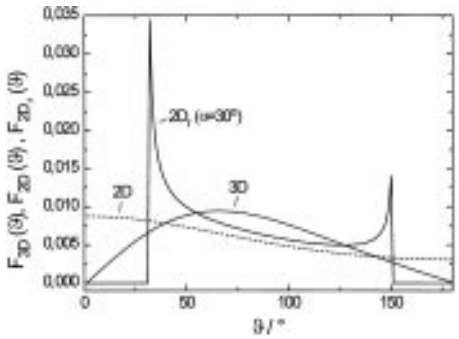

Figure 3. Plot of the three orientational distribution functions $F_{3D}(\vartheta)$, $F_{2D}(\vartheta)$, and $F_{2Dr}(\vartheta)$.

$\vec{e}_Z$ and $\vec{e}_\mu$ are the unit vectors along the z-axis and the direction of the dipole moment, respectively. e_Z and e_μ are the absolute values of the corresponding vectors.

Figure 2 shows a plot of φ as a function of ϑ with $\alpha = 30°$ (see below). Without an applied electric poling field the molecules are isotropically distributed over φ. Equally sized segments $\Delta\varphi$ contain the same number of molecules. Since φ is a nonlinear function of ϑ, the chromophores are no longer equally distributed with respect to the variable ϑ. The probability of finding molecules in a particular angle segment $\Delta\vartheta$ is proportional to the local gradient of the function $\varphi(\vartheta)$ in this interval:

$$\frac{\partial \varphi}{\partial \vartheta} = \frac{\sin \vartheta}{(\cos^2 \alpha - \cos^2 \vartheta)^{1/2}} \quad (7)$$

Therefore, the distribution function $F_{2D,r}(\vartheta, E)$ is given by

$$\int_0^\pi F_{2D,r}(\vartheta, E) \, d\vartheta = K''' \int_0^\pi \frac{\sin \vartheta}{(\cos^2 \alpha - \cos^2 \vartheta)^{1/2}} e^{m \cos \vartheta} \, d\vartheta \quad (8)$$

The main features of the different dimensional restrictions can be understood from the plot of the total weighting functions $F(\vartheta, E)$ versus ϑ (Figure 3). The restriction by one dimension [case (b) versus case (a)] induces a significant redistribution of the orientational function to smaller angles parallel to the z-axis. The additional restriction by the tilt angle α will, however, prevent molecules from entering the angular segments between $0° < \vartheta < \alpha$ and $180° - \alpha < 9 < 180°$. These features have profound effects on the tensor components of the nonlinear optical susceptibility $\chi^{(2)}$. Parts a and b of Figure 4 compare the polar order parameters $\langle \cos^3 \vartheta \rangle$ and $0.5 \langle \sin^2 \vartheta \cos \vartheta \rangle$, as a function of the poling field E_{pol} for the three configurations. Here and in the following α is set to 30°. The dimensional restriction [case (b)] leads to an enhancement in $\chi^{(2)}_{ZZZ}$ by a factor of close to 2 compared to the 3D case. This effect is

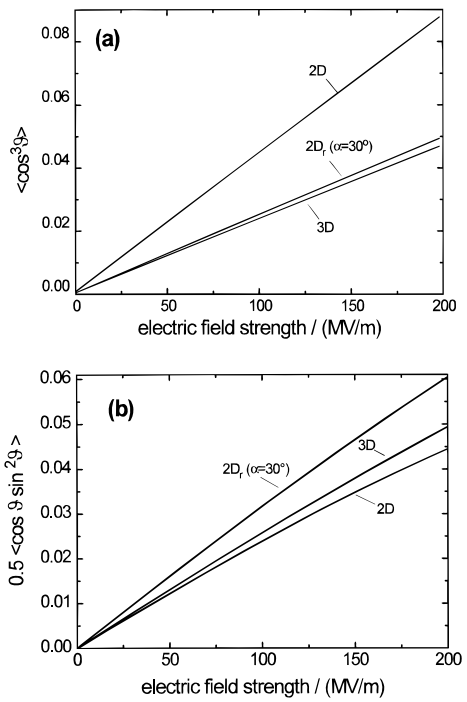

Figure 4. (a) Comparison of the polar order parameter $\langle\cos^3 \vartheta\rangle$ as a function of the electric poling field. (b) Comparison of the polar order parameter $\langle 0.5 \cdot \cos \vartheta \sin^2 \vartheta\rangle$ as a function of the electric poling field for the three different distribution functions.

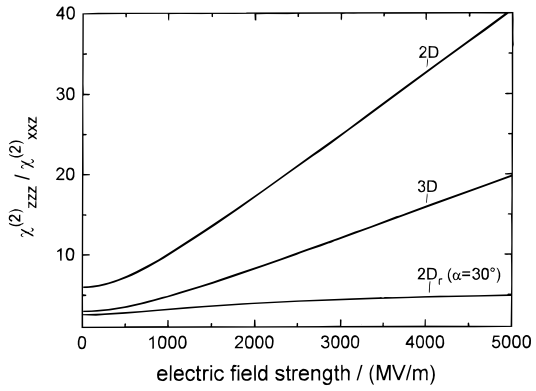

Figure 5. Dependence of the ratio $\chi^{(2)}_{ZZZ}/\chi^{(2)}_{XXZ}$ on the electric field strength of the poling field.

reduced if $\alpha \neq 0$ [case (c)]: $\chi^{(2)}_{ZZZ}$ is only increased by approximately 10%. At the same time $\chi^{(2)}_{XXZ}$ is enhanced by a factor of around 1.4 The two tensor components become more equal in comparison with the 2D and 3D cases. This illustrates that the ratio between $\chi^{(2)}_{ZZZ}$ and $\chi^{(2)}_{XXZ}$ can be adjusted by fixing α to a certain angle. Comparable values of both tensor components might become necessary for the modulation of unpolarized light in an electrooptical waveguide device. The ratios at low poling fields are

$$(\chi^{(2)}_{ZZZ}/\chi^{(2)}_{XXZ})_{3D} \cong 3, \quad (\chi^{(2)}_{ZZZ}/\chi^{(2)}_{XXZ})_{2D} \cong 6,$$
$$(\chi^{(2)}_{ZZZ}/\chi^{(2)}_{XXZ})_{2D,r} \cong 2.5$$

For larger poling fields this ratio will also depend on the field strength E_{pol} as shown in Figure 5, but again the correlation is strongly effected by dimensional restrictions. It is worth noting that the ratios for the 3D and 2D cases tend to approach infinity when the electric field is increased, whereas for the $2D_r$ case a limited value of 6 (with $\alpha = 30°$) is reached.

It should be noted that an isotropic distribution of the rigid rod backbones in all three directions, omitting the layered structure suggested in Figure 1b,c, would lead to a distribution function identical to the three dimensional case (a).

With regard to technical applications of poled polymers, the relaxation characteristics of the polar order after the poling field has been switched off will now be discussed in more detail. Orientational relaxation has often been described within the framework of rotational diffusion.[3–5] This is particularly applicble for temperatures below the glass transition temperature, where the relaxation is dominated by small-angle jumps. We first review the well known three dimensional case (a), which has been extensively treated by Wu.[4] The rotational diffusion equation in the absence of an external potential is given by

$$\frac{\partial F(t, i, j, k)}{\partial t} = D\Delta F(t, i, j, k) \tag{9}$$

with D being the rotational coefficient and Δ the Laplace operator in polar coordinates

$$\Delta_{3D}(\vartheta) \equiv \frac{\partial^2}{\partial \vartheta^2} + \cot \vartheta \frac{\partial}{\partial \vartheta} \tag{10}$$

Because the Legendre polynomials $P_n(\vartheta)$ are eigenfunctions of this operator, it is common to expand the orientational function into a series of P_n's, namely:

$$F_{3D}(\vartheta) = \sum_{n=0}^{\infty} \frac{2n+1}{2} A_n P_n(\cos \vartheta) \tag{11}$$

Under the poling field the first three nonzero coefficients of the Boltzmann-weighted distribution function in eq 4 become

$$A_0(t=0) = 2$$
$$A_1(t=0) = \frac{1}{3}\left(2m + \frac{m^3}{9}\right)$$
$$A_3(t=0) = \frac{2m^3}{63} \tag{12}$$

Combining 2.11 and 2.12 with 2.9 and applying the well-known relation

$$\Delta_{3D} P_n(\cos \vartheta) = -n(n+1) P_n(\cos \vartheta) \tag{13}$$

give

$$\frac{\partial A_n(t)}{\partial t} = -Dn(n+1) A_n(t) \tag{14}$$

With $A_n(t=0)$ being the nth coefficient of the polar order at the time the poling field is switched off (eq 12), the analytical solution of the time-dependent distributional function under rotational relaxation reads

$$F_{3D}(\vartheta, t) = 1 + \frac{1}{2}\left[\left(2m + \frac{m^3}{9}\right)e^{-2Dt} - \frac{m^3}{9} e^{-12Dt}\right] \cos \vartheta + \frac{m^3}{6} e^{-12Dt} \cos^3 \vartheta \tag{15}$$

The decay of the polar order is mainly described by a single exponential decay of a lifetime of $t = 1/(2D)$ (note that $2m \gg (m^3)/9$, $(m^3)/6$ for $m \ll 1$).

For the two dimensional case (b) the rotational diffusion will only occur along a circle described by the angle φ. The restriction is reflected in a modified Laplace operator:[3,4]

$$\Delta_{2D}(\vartheta) = \frac{\partial^2}{\partial \vartheta^2} \tag{16}$$

The orientational function can now be expanded in a Fourier series:[6]

$$F_{2D}(\vartheta) = \sum_{n=0}^{\infty} 2C_n \cos n\vartheta \tag{17}$$

with the first three nonzero coefficients

$$C_0(t=0) = 1/2$$

$$C_1(t=0) = \frac{m}{2} + 3C_3(t=0) = \frac{m}{2} + \frac{m^3}{16}$$

$$C_3(t=0) = m^3/48 \tag{18}$$

With the eigenwert relation

$$\Delta\cos(n\vartheta) = -n^2 \cos(\mathrm{n}\vartheta) \tag{19}$$

the time evolution of the nth coefficient is given by

$$\frac{\partial c_n(t)}{\partial t} = -Dn^2 c_n(t) \tag{20}$$

This leads to the final result for the two dimensional case:

$$F_{2D}(\vartheta, t) = 1 + \left[\left(m + \frac{m^3}{8}\right)e^{-Dt} - \frac{m^3}{8}e^{-9Dt}\right]\cos\vartheta + \frac{m^3}{6}e^{-9Dt}\cos^3\vartheta \tag{21}$$

Again, the decay of the polar order is dominated by a single exponential. However, the restriction by one dimension will reduce the relaxation rate by a factor of about 2 (note that the main term is $m \exp(-Dt) \cos\vartheta$ for $m \ll 1$). The case (c) can be included into the formulas for case (b) by simply replacing the factor m with

$$m' = m \cos\alpha \tag{22}$$

Finally, the relevant angular averages in (1) can be computed, yielding

$$\langle(\cos^3\vartheta)(t)\rangle_{3D} = \left(\frac{1}{5}m + \frac{1}{90}m^3\right)e^{-2Dt} + \frac{4}{315}m^3e^{-12Dt} \tag{23}$$

$$\langle(\cos\vartheta \sin^2\vartheta)(t)\rangle_{3D} = \left(\frac{2}{15}m + \frac{1}{135}m^3\right)e^{-2Dt} + \frac{2}{945}m^3e^{-12Dt} \tag{24}$$

and

$$\langle(\cos^3\vartheta)(t)\rangle_{2D} = \left(\frac{3}{8} + \frac{3}{64}m^2\right)me^{-Dt} + \frac{m^3}{192}e^{-9Dt} \tag{25}$$

$$\langle(\cos\vartheta \sin^2\vartheta)(t)\rangle_{2D} = \left(\frac{1}{8} + \frac{1}{64}m^2\right)me^{-Dt} - \frac{m^3}{192}e^{-9Dt} \tag{26}$$

By considering the trigonometric identities

$$\langle\cos^3\vartheta\rangle = \cos^3\alpha\langle\cos^3\varphi\rangle \tag{27a}$$

and

$$\langle\cos\vartheta \sin^2\vartheta\rangle = \cos^3\alpha\langle\cos\varphi \sin^2\varphi\rangle + \cos\alpha \sin^2\alpha\langle\cos\varphi\rangle \tag{27b}$$

the averages for the $2D_r$ case can be calculated

$$\langle(\cos^3\vartheta)(t)\rangle_{2D_r} = \cos^3\alpha\left[\left(\frac{3}{8} + \frac{3}{64}(m')^2\right)(m')e^{-Dt} + \frac{(m')^3}{192}e^{-9Dt}\right] \tag{28}$$

$$\langle(\cos\vartheta \sin^2\vartheta)(t)\rangle_{2D_r} = \left[\left(\frac{1}{8} + \frac{(m')^2}{64}\right)(4 - 3\cos^2\alpha)\right](m')\cos\alpha e^{-Dt} - \frac{(m')^3\cos^3\alpha}{192}e^{-9Dt} \tag{29}$$

The time evolutions of $\langle\cos^3\vartheta\rangle$ plotted in Figure 6 prove a remarkable improvement purely through the dimensional restriction of the distribution function. For $m \ll 1$ (small poling fields) and $t = 0$, (23) and (24) reduce the well-known relations for poled polymer films.[2] The decay of both tensor components $\chi^{(2)}_{zzz}$ and $\chi^{(2)}_{xxz}$ occurs with the same relaxation rate, which is $2D$ in the three dimensional case and D for the two dimensional geometries (b) and (c), in agreement to similar calculations by Wu and Firestone et al.[4]

Experimental Section

Linear and Nonlinear Optical Measurements. Optical UV−vis spectra were recorded on a Lambda 9 photospectrometer.

Linear and nonlinear optical susceptibilities of polymer films were measured by the attenuated total reflection (ATR) method. Samples for the ATR setup were prepared as follows: A 6−10% polymer−tetrachloroethane solution was spin-coated onto a 40-nm-thick gold layer that had been previously evaporated on a BK7 glass slide. Typical polymer film thicknesses obtained at a spinning rate of 1000 rpm at 50−80 °C were 2 μm (depending on the concentration) solution. The films were dried i.v. and a 100-nm-thick gold top electrode was evaporated on top of the layered structure. The dried films were poled by applying an electric field between the two gold electrodes. Poling conditions were as follows: poling fields, 40−60 V/mm; temperature, 185−195 °C; poling time, 10 min; cooling rate (with applied field), 0.2 °C/min.

In an ATR experiment the reflectivity of the multilayer system is recorded as a function of the incident angle. At specific angles light is coupled into waveguide modes; resulting in significant dips in the reflectivity spectrum. Analysis of these features by a Fresnel formalism yields the tensor components of the linear dielectric tensor as well as the thickness of the polymer films. s- and p-polarized light can be used to address the different tensor components ϵ_{YY} (s-polarization) as well as ϵ_{XX} and ϵ_{ZZ} (p-polarization). Here, the

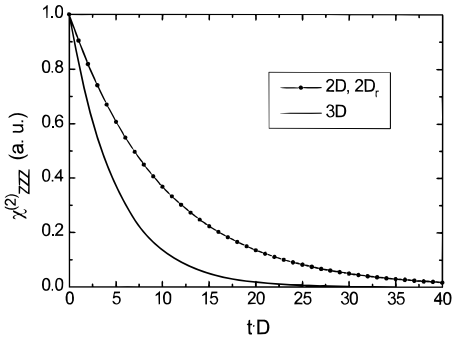

Figure 6. Plot of the time evolution of $\langle \cos^3 \vartheta(t) \rangle$ for the 3D, 2D, and 2D$_r$-distribution according to eqs 23, 25, and 28.

z-axis is defined as being perpendicular to the film plane with light incident in the *xz*-plane.

After poling along the *z*-direction, the external field E_Z will induce a change in the dielectric tensor components due to the Pockels effect:

$$\epsilon_{JJ}(E_Z) = \epsilon_{JJ}(0) + 2\chi^{(2)}_{JJZ}E_Z + o(E_Z^n) \tag{30}$$

with $o(E_Z^n)$ being the higher order terms neglected in this approach. In addition, the frozen-in polarization P_f will cause a piezoelectric effect:

$$h(E_Z) = h(0)(1 + d_{ZZ}E_Z + o(E_Z^n)) \tag{31}$$

where the piezoelectric tensor component d_{zz} is given by[7]

$$d_{ZZ} = -K_{plate}P_f\left(\frac{\epsilon + 2}{3} - \frac{2}{5}\right) \tag{32}$$

K_{plate} is the effective mechanical compressibility of the thin polymer film and ϵ the dielectric function. The elastic deformation will further alter the chromophore number density and by this effect the linear optical properties through the Clausius−Mussotti relation:

$$\frac{\partial \epsilon}{\partial h} = -\frac{(\epsilon + 2)(\epsilon - 1)}{3h} \tag{33}$$

Finally, the total change in reflectivity R due to the external electric field is given by

$$\frac{\partial R}{\partial E_Z} = \frac{\partial R}{\partial \epsilon_{YY}}\frac{\partial \epsilon_{YY}}{\partial E_Z} + \frac{\partial R}{\partial h}\frac{\partial h}{\partial E_Z} + \frac{\partial R}{\partial \epsilon_{YY}}\frac{\partial \epsilon_{YY}}{\partial h}\frac{\partial h}{\partial E_Z} \tag{34}$$

for s-polarized light and

$$\frac{\partial R}{\partial E_Z} = \frac{\partial R}{\partial \epsilon_{XX}}\frac{\partial \epsilon_{XX}}{\partial E_Z} + \frac{\partial R}{\partial \epsilon_{ZZ}}\frac{\partial \epsilon_{ZZ}}{\partial E_Z} + \frac{\partial R}{\partial h}\frac{\partial h}{\partial E_Z} + \frac{\partial R}{\partial \epsilon_{XX}}\frac{\partial \epsilon_{XX}}{\partial h}\frac{\partial h}{\partial E_Z} + \frac{\partial R}{\partial \epsilon_{ZZ}}\frac{\partial \epsilon_{ZZ}}{\partial E_Z}\frac{\partial h}{\partial E_Z} \tag{35}$$

for p-polarization of the incident light. Modulated reflectivity spectra are recorded as a function of the incidence angle. The fit according to eqs 34 and 35 yields the $\chi^{(2)}$ tensor components $\chi^{(2)}_{ZZZ}$, $\chi^{(2)}_{XXZ}$, and $\chi^{(2)}_{YYZ}$ as well as the piezoelectric constant d_{ZZ}. The temporal decay of the polar order could be followed in situ by performing successive modulated scans over a dominant waveguide mode while the sample was kept at a fixed temperature with no poling field applied. Time constants were obtained by fitting the maximum modulation amplitude as a function of time to bi- or triexponential decay curves. The ATR setup and the detailed analysis are published elsewhere.[8,9]

Results and Discussion

The UV region of the linear absorption of the chromophore bearing polymers is dominated by the absorption at 320 nm caused by the poly(esteramide) backbone. The presence of the NLO chromophore is indicated by the shoulder at around 374 nm (Figure 7), which is close to the absorption maximum of 4-nitro-*N*,*N*-dimethylaniline (PNA) in dioxane.[10]

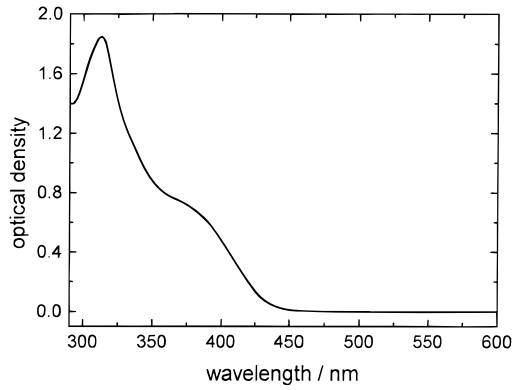

Figure 7. Absorption spectrum of a 0.4 μm thick film of **P3**.

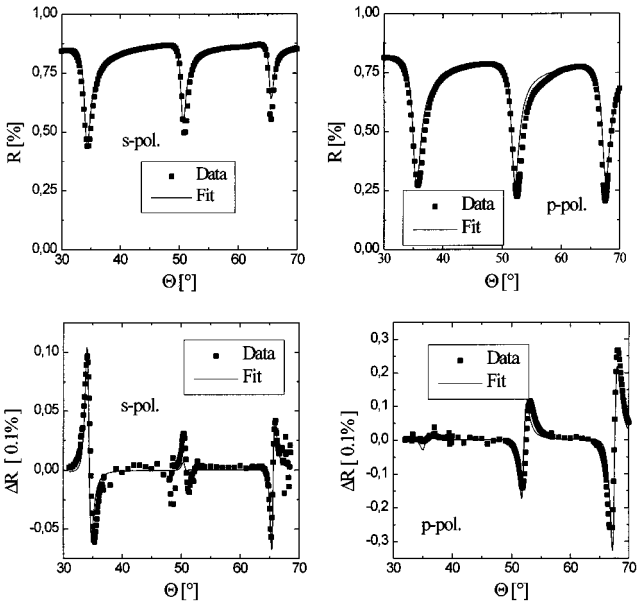

Figure 8. Reflectivity (upper figures) and modulated reflectivity (lower figures) as a function of the incident angle for a 1.9-mm-thick film of polymer **P2a** for two polarizations of the incident light. The solid lines are best fits according to a Fresnel formalism for deriving the linear and electrooptical coefficients.

Table 1. (a) Linear and (b) Nonlinear Optical Coefficients of a Spin-Coated Film of Polymer P2a As Derived from ATR Scans

a			
ϵ_{XX}	ϵ_{YY}	ϵ_{ZZ}	h/μm
2.660	2.685	2.610	1.83
b			
$\chi^{(2)}_{XXZ}$/pmV^{-1}	$\chi^{(2)}_{YYZ}$/pmV^{-1}	$\chi^{(2)}_{ZZZ}$/pmV^{-1}	d/pm V^{-1}
0.02(2)	0.02(2)	0.9(2)	−0.4

Figure 8 (upper figures) shows the s- and p-polarized ATR scans for a 1900-nm-thick sample of polymer **P2a**. The linear optical parameters deduced from these scans are listed in Table 1.

Poling of the sample at 40 V/μm did not greatly effect the linear optical parameters. The modulated ATR scans of the same film after poling are shown in Figure 8 (lower figures) for two different polarizations of the incident laser light. One observes competitive contribu-

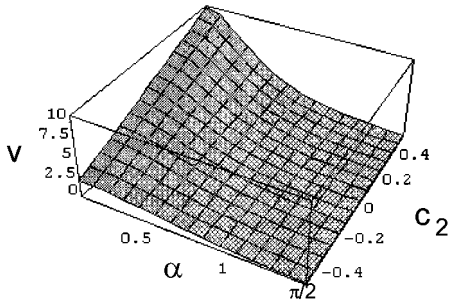

Figure 9. Dependence of the ratio $v = \chi^{(2)}_{ZZZ}/\chi^{(2)}_{XXZ}$ on the tilt angle α (Figure 1) and the parameter c_2 defined in eq 36.

tions from the electrooptical and piezoelectrical effect, revealed in the inverse course of modulation signals at 35° and 66° as well as the minor modulation of the central mode in the s-polarized configuration. Similar modulation patterns were observed for all polymer samples (**P2a**, **P2b**, **P3**). The s-polarized modulation signal is almost entirely fitted by the piezoelectric effect, with small contributions from $\chi^{(2)}_{XXZ}$, while the stronger modulation of the reflectivity for p-polarized light is explained by a larger $\chi^{(2)}_{ZZZ}$ value (assuming the same value for $\chi^{(2)}_{XXZ}$ and $\chi^{(2)}_{YYZ}$. Independent interferometrical experiments were carried out in order to establish the electromechanical contribution.[7] A piezoelectric coefficient of $d_{33} = -1$ pm/V was found for a film of **P2b** poled at 100 V/μm, corresponding to −0.4 pm/V for E_{pol} = 40 V/μm. The nonlinear optical parameters as determined from the modulated ATR scans are summarized in Table 1.

The ratio $\chi^{(2)}_{ZZZ}/\chi^{(2)}_{XXZ}$, which is clearly above 6, is not solely explained by the theory presented above, even if the tilt angle α were close to 0°. In general one would assume an anisotropic potential $U(\varphi)$ describing the rotation of the chromophore around the main chain axis. Since the exact characteristics of this potential are unknown, we used a phenomenological description of the rotational distribution $F(\varphi)$ in the unpoled state by a Fourier expansion:

$$F(\varphi, E_{pol} = 0) = 1 + 2c_2 \cos(2\varphi) \qquad (36)$$

For simplicity, higher order Fourier coefficients were neglected in the following even though they become important in highly ordered geometries.[11] For $c_2 > 0$ the chromophore will be preferentially aligned parallel to the *z*-axis. $c_2 < 0$ describes a preferential orientation of the chromophore parallel to the substrate plane. Figure 9 shows the ratio $v = \chi^{(2)}_{ZZZ}/\chi^{(2)}_{XXZ}$ as a function of the tilt angle α and the parameter c_2. The range for *v* is now extended to larger values. While an exact analysis is not possible without knowing the degree of main chain alignment, this consideration indicates a particular geometry of the main chains in the film with a preferential orientation of the chromophore perpendicular to the substrate. It is important to note that the applied analysis (eqs 34 and 35) of the modulated ATR scans as outlined above relies on the isotropy of the optomechanical tensor:

$$\sigma_{JJ} = \frac{\partial \epsilon_{JJ}}{\partial h} \qquad (37)$$

This assumption cannot be generalized to the present case of a strongly anisotropic structure. Therefore, the anisotropy of the electrooptical response as deduced from the given analysis might be falsified by electromechanical effects.[12]

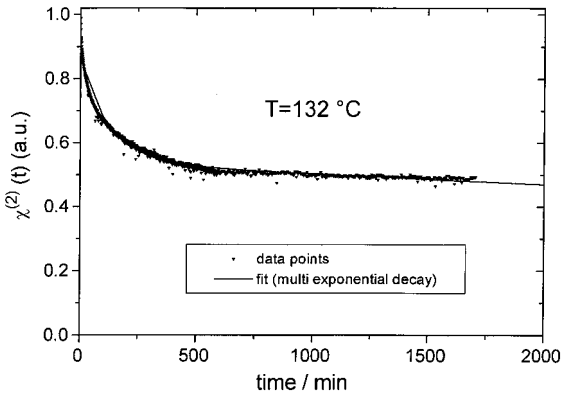

Figure 10. Example of the long term stability of the electrooptical effect measured with the ATR method for polymer **P3** at 132 °C.

Strong piezoelectric contributions can be expected in materials with a high compressibility or if chromophores with large ground state dipole moments μ_g and rather small hyperpolarizabilities β, as in the case of PNA, are used. The bulk compressibilities of our systems as determined from electrostriction experiments showed values which are typically found in the polymeric glasses below the glass transition temperature. Rough estimations of the electrooptical coefficient $\chi^{(2)}_{ZZZ}$ and piezoelectric contribution d_{ZZ} for the 3D geometry were derived from[2,7]

$$\chi^{(2)}_{ZZZ} = N f_\omega^2 f_o \beta_{zzz} \frac{\mu_g E_{pol} f_o}{5kT_{pol}} \cong 0.7 pm/V \qquad (38)$$

$$d_{ZZ} = -K_{plate} N \mu_g f_\omega \left(f_\omega - \frac{2}{5}\right) \frac{\mu_g E_{pol} f_o}{3kT_{pol}} \cong -0.35 pm/V \qquad (39)$$

using $N = 5 \times 10^{20}$ cm^{-3}, $\beta_{zzz} = 29 \times 10^{-30}$ esu, $\mu_g = 7.1$ D, $f_\omega f_o = 1.43$, $E_{pol} = 40$ V/μm, $T_{pol} = 473$ K, and a plate compressibility K_{plate} of 2.7×10^{-10} Pa^{-1}.[10,13] (The value for the number density *N* was determined by comparing the optical density of solutions of **14** in DMSO of known concentration with the optical density of the prepared films.) In agreement with the experimental data, both contributions are of comparable size.

Figure 10 shows the temporal stability of the nonlinear optical susceptibility at elevated temperature. A clear multiexponential decay of the electrooptical signal was observed for all temperatures. More than 50% of the modulated intensity is still retained after 30 h, even at 132 °C. The relaxation parameters deduced from the multiexponential fits to the polar relaxation experiments are summarized in Table 2.

Note that up to three relaxation times had to be used to characterize the decay of **P2b** and **P3** sufficiently while the relaxation data of **P2a** could be fitted according to a biexponential decay (with time constants τ_2 and τ_3). This partly explains the difference in the relaxation rates of polymer **P2a** and **P2b**. On the other hand, this difference might be caused by different molecular weights or weight distributions resulting from the preparation conditions described in ref 1. While the longest time constant τ_3 of the multiexponential fit decreases monotonically with increasing temperature, the behavior of the shorter time constants is less

Table 2. Relaxation Times τ_n for P2a/b and P3 derived from Multiexponential Fits to the Polar Relaxation Data ("–" not measured, nd not determined)

	P2a		P2b			P3		
temp/deg	τ_2/h	τ_3/h	τ_1/h	τ_2/h	τ_3/h	τ_1/h	τ_2/h	τ_3/h
85	n.d.	498(54)	–	–	–	–	–	–
101	3.1(1)	120(4)	–	–	–	0.160(4)	8.1(1)	833(25)
108	–	–	–	–	–	n.d.	3.9(7)	749(137)
116	0.73(8)	98(6)	–	–	–	0.44(2)	12.3(9)	411(121)
124	–	–	1.8(1)	17(2)	408(62)	1.8(1)	17(2)	408(62)
132	0.73(1)	41(4)	–	–	–	–	–	–
140	–	–	0.766(4)	12.2(3)	231(9)	–	–	–

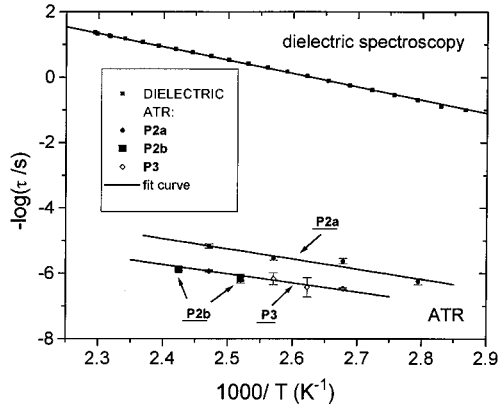

Figure 11. Comparison of the longest relaxation rates τ_3 in Table 2 for the polymers **P2a**, **P2b**, and **P3** measured with the ATR setup with the data derived from the dielectric measurements shown in Figure 7 in ref 1 in an Arrhenius-type plot.

Table 3. Activation Energies of the Polymers P2a and P3 Determined from Electrooptical And Dielectric Measurements (Figure 11)

method	ATR	dielectric[1]	ATR
polymer	**P2a**	**P2a**	**P3**
E_A, kJ/mol	59(10)	77.9(7)	54(8)

consistent. This indicates that more than one physical relaxation process is involved in the decrease of the electrooptical response over time. In fact, it was not possible to fit the decay curves with a continuous Kohlrausch–Williams–Watts (KWW) or a Havriliak–Negami distribution of relaxation times. On the contrary, isothermal polar decay data of rigid-rod-like polymers with the EO-active chromophore linked to the main chain by a flexible spacer could be well fitted by a continuous distribution of relaxation times. In this case, a discrete distribution could be even excluded based on thermally stimulated discharge current experiments.[14]

The molecular origin of the polar relaxation can be partly understood from a plot of the longest time constant τ_3 as a function of the temperature. Figure 11 compares the relaxation rates for polymers **P2a**, **P2b**, and **P3** in an Arrhenius-type representation together with the relaxation data derived from dielectric spectroscopy on polymer **P2a** (see ref 1). In all systems log(τ) is linear with $1/T$. The fit to

$$-\log(\tau) = -\log(\tau_o) + \frac{E_a}{\ln 10 kT} \qquad (40)$$

gives activation energies of about 60 kJ/mol (Table 3). It is worthwhile noting that polymer **P2** and polymer **P3** (with hexyloxy and dodecyloxy side chains, respectively) show the same thermal activation energy of the relaxation process. It can be concluded that the relaxation is dominated by a rotation of the chromophore around the amide bond and does not include the rotation of the whole "trimer" structure or even larger blocks.

The rotational motion of para linked phenyl rings has been studied extensively by ^{2}H-NMR spectroscopy in the solid state for different polymers. For liquid crystalline polymers with unsubstituted phenyl benzoate moieties as mesogenic side groups, motionally narrowed spectra corresponding to a 180° flip around the para axis appeared in one dimensional ^{2}H-NMR experiments at temperatures between 240 and 300 K.[15] The temperature dependence of correlation times showed clearly a locally activated Arrhenius-like behavior with activation energies in the range 42–47 kJ/mol. Similar results were obtained for the rotational motion of deuterated stilbenol NLO chromophores in the side group of electrooptic active polymers.[16,17] In rigid-rod-like aromatic polyesters, a 180° flip of the unsubstituted hydrochinone became visible in the NMR spectra above a temperature of around 260 K.[18] Additional narrowing due to the onset of a diffusive uniaxial rotation around the para bond was observed at higher temperatures. For the alkyl substituted terephthalic acid unit, no indication of a 180° flip of the phenyl ring can be deduced from the 1D-^{2}H-NMR spectra. The onset of the isotropic rotation can be clearly correlated with specific mesophase transitions. This is in further agreement with results on deuterated hydroquinone units bearing long NLO-active side groups in the meta position.[19] In these systems the uniaxial rotational diffusion is observed either upon the phase transition from a smectic-like to a nematic-like morphology or even upon melting. The effect of substitution on the phenylene motion was further investigated for polycarbonate.[20] The substitution of methyl groups at the ortho position of the rings raises the onset of the fast 180° ring flip by around 180 K. Correlation times below 10^{-4} are now only observed at temperatures above 400 K.

For our systems with very bulky dimethylamino and nitro substituents, significant reduction of the ring mobility can be expected. The relaxation process found by dielectric spectroscopy with relaxation rates of approximately 1 s might thus be associated with a 180° flip of the PNA-type chromophore. This is further corroborated by the large dielectric strength which is correlated with the relaxation process as mentioned before. An assignment of the motion causing the polar relaxation is aggravated by the difference between the polar relaxation times and the results from dielectric spectroscopy (Figure 11). The large difference of several orders in time as well as the multiexponential decay behavior as displayed in Figure 10 indicates that the processes observed by dielectric spectroscopy and polar decay experiments represent two different relaxation mechanisms. Smaller discrepancies had been frequently observed in other relaxation experiments on glass forming polymers.[21–23] In some of these cases the

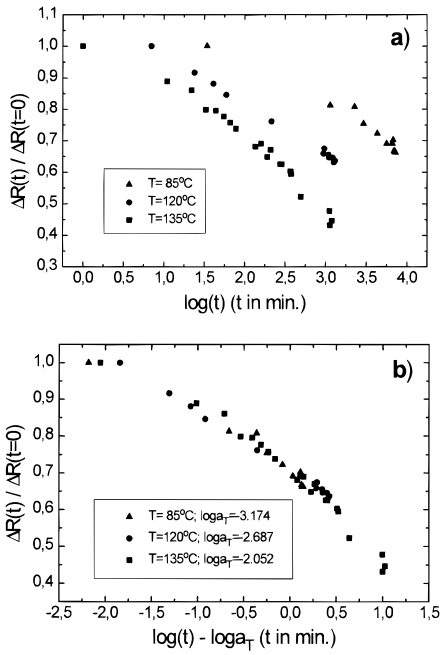

Figure 12. (a) Electrooptical signal as a function of log(t), normalized with respect to the signal at $t = 0$. (b) Data from Figure 12a but shifted horizontally to form a master curve.

difference in relaxation times could be explained by different thermal treatments of the sample during the dielectric and polar relaxation experiments.[24]

Figure 12a shows the electrooptical signal as a function of log(t) for polymer **P2a** measured at three different temperatures. The shape of the decay curves already indicates that the time−temperature superposition principle is fulfilled. In fact the curves obtained at different temperatures can be shifted horizontally to form a master curve as shown in Figure 12b. The superposition principle is usually best fulfilled in the viscoelastic region but large deviations are generally observed in the glassy state of polymeric materials.[25] This observation implies that the polar relaxation for our systems is not coupled to a glass transition.

The picture of a locally activated relaxation process is in agreement with the results from dielectric spectroscopy, showing only a time-temperature dependence typical for a local β-relaxation process. These results indicate that the motion of the chromophore is decoupled from the dynamics in the side chain region due to the microphase separation. On the basis of further results published elsewhere, we presume that locally activated chromophore relaxation is a common phenomenon in layered structures of rigid rod main chain polymers with chromophores rigidly linked to the main chain.[12,26] It is especially noteworthy that a temperature dependent decoupling of dopant motion from the behaviour of the host polymer has been argued recently in order to explain the Arrhenius-type time−temperature characteristics even for a 1 wt % guest−host system of 4-(dimethylamino)-4′-nitrostilbene (DANS) in poly(ethyl methacrylate) below the glass transition temperature.[23] An Arrhenius temperature dependence of relaxation has been also observed by studying the reorientation dynamics of disperse red 1 (DR1) chromophores doped at 2 wt % in polystyrene.[27] However, non-Arrhenius-type time−temperature characteristics seem to prevail for guest−host or side chain polymer systems based on flexible polymer main chains.[28] Recently, simulations of polar relaxation data based on the Adam−Gibbs theory indicated that non-Arrhenius-type activation of polar relaxation should be generally observed in glass forming polymers, provided a sufficiently strong coupling of the chromophore motion to the dynamics of the polymer host.[24]

At this point, it is necessary to recognize that our concept differs significantly from other recently published approaches using main chain polymers for second order nonlinear optics.[29−35] In many of those systems, the chromophore donor−acceptor axis lies parallel to the main chain direction. This implies that the predominant chromophore relaxation is always coupled to a nonlocal relaxation of the main chain. Further, Weder et al. have published EO-active polyamides based on 2′,5′-diamino-4-(dimethylamino)-4′-nitrostilbene and linear aliphatic diacid chlorides.[34] In contrast to our systems, the incorporation of flexible spacers reduces the stiffness of the polymer chains. As a consequence such polymers show a clear glass transition and the polar relaxation could be correlated to T_g.[35]

Conclusions

The electrooptical properties and relaxation behavior of rigid-rod-like main chain poly(ester amide)s with long flexible alkoxy side chains and rigidly attached NLO-active chromophores have been thoroughly investigated. Regarding the correlation between the structural data (see ref 1) and the macroscopic nonlinear optical susceptibility, theoretical calculations showed the following: (1) Depending on the angle between the dipole axis of the chromophore and the direction of the poling field, high values of $\chi^{(2)}_{zzz}$ can be expected. This enhancement is greater (in comparison with "flexible systems"), if the chromophore can be oriented into a fully upright, perpendicular position with respect to the main chain (2D-case).

(2) The restriction of the chromophore to a two dimensional mobility increases the theoretical relaxation times by a factor of 2 compared to systems with flexible main chains.

(3) The quotient $\chi^{(2)}_{zzz}/\chi^{(2)}_{xxz}$ can be strongly influenced by the bonding angle of the chromophore. Furthermore, the influence of neighboring side chains or of sterical hindrance on the orientation of the chromophore could be simulated by assuming an anisotropic potential (nematic potential).

The time dependent measurements of the EO effect for various temperatures revealed a thermal stability superior to that of most non-cross-linked polymer materials. In combination with dielectric measurements the relaxation process has been assigned to the two dimensional rotation of the *N*,*N*-dimethylamino-4-nitroterephthalic acid moiety. The relaxation process exhibits a thermally-activated Arrhenius behavior with an activation energy of approximately 60 kJ/mol. It is worth stressing that this behavior is completely different from that of glassy polymers (e.g., the well-known PMMA derivatives). The relaxation process in these systems can often be described by a WLF equation with relaxation times in the range of seconds when the system is heated close to the glass transition temperature.

The large $\chi^{(2)}_{zzz}/\chi^{(2)}_{xxz}$ quotient clearly demonstrates the anisotropic structure of the measured films. The chromophores are preferentially aligned perpendicular to the main chain and the substrate surface. For all investigated films, the $\chi^{(2)}_{xxz}$ coefficients were consistently very small (0.02−0.05 pm/V). In contrast, the range of the

$\chi^{(2)}_{zzz}$ values derived from different films varied considerably. The largest $\chi^{(2)}_{zzz}$ value was around 2 pm/V, leading to an enhancement by a factor of approximately 2 compared to the theoretical value calculated for a flexible system (eq 38). This would be in agreement with our theory. However, a direct comparison between theory and experimental values is hampered for several reasons: due to the rather low hyperpolarizability of the PNA chromophore, the influence and interdependence of the piezoeffect on the evaluation of the NLO coefficient has to be considered. It is a general conclusion of this paper that the determination of EO coefficients without consideration of the electromechanical effects must lead to incorrect NLO values and therefore to a false description and interpretation of the investigated systems. Furthermore, some of data (local field factors, number density, etc.) used to evaluate the NLO coefficient cannot be determined with sufficient accuracy, so that it is very difficult to validate our theory with respect to absolute values. The low average value of the $\chi^{(2)}_{zzz}$ coefficient of around 0.7 pm/V might be also explained by an insufficient poling: a large number of chromophores are still of antiparallel orientation. This conclusion is corroborated to some extent by the few (reproducible) measurements leading to larger $\chi^{(2)}_{zzz}$ coefficients. Obviously, a more efficient poling with a better alignment of the chromophores must have taken place in these cases. Higher nonlinear coefficients can be expected by improving the polymer structure with regard to the number density of the chromophores and the molecular hyperpolarizability of the chromophores and by applying higher poling fields.

Finally, it should be mentioned that several films were investigated over a period of 1−2 years and were poled and unpoled without any signs of decomposition or decay as long as the measurements at higher temperatures were performed under inert gas conditions.

Acknowledgment. This work was financially supported by the German ministry of research and technology (BMFT) under the project 03 M 4046. We gratefully acknowledge Dr. M. Schulze for fruitful discussions.

References and Notes

(1) Heldmann, C.; Neher, D.; Winkelhahn, H.-J.; Wegner, G. *Macromolecules*, preceding paper in this issue.
(2) Singer, K. D.; Kurzyk, M. G.; Sohn, J. E. In *Nonlinear Optical and Electroactive Polymers*; Prasad, P. N., Ulrich, D. R., Eds.; Plenum Press: New York, 1988; p 189.
(3) Marrucci, G.; Maffettone, P. L. *Macromolecules* **1989**, *22*, 4076.
(4) a) Wu, J. W. *J. Opt. Soc. Am. B* **1991**, *8*, 142. (b) Firestone, M. A.; Ratner, M. A.; Marks, T. J. *Macromolecules* **1995**, *28*, 6296.
(5) Kivelson, D.; Kivelson, S. A.; *J. Chem. Phys.* **1989**, *90*, 4464.
(6) Neher, D.; Mittler-Neher, S.; Cha, M.; Stegeman, G. I.; Embs, F. W.; Wegner, G.; Miller, R. D.; Willson, C. G. *Proc. SPIE* **1991**, *1560*, 335.
(7) Winkelhahn, H.-J.; Winter, H. H.; Neher, D. *Appl. Phys. Lett.* **1994**, *64*, 1347.
(8) Dumont, M.; Levy, Y.; Morichere, D. In *Organic Molecules for Nonlinear Optics and Photonics*; Messier, J., et al., Eds.; Kluwer Academic Publishers: Dodrecht, 1991; NATO ASI Series E, Vol. 194, p 461.
(9) Aust, E. F.; Ito, S.; Sawodny, M.; Knoll, W. *Trends Polym. Sci.* **1994**, *2*, 313.
(10) Parley, M. S.; Harris, J. M.; Looser, H.; Baumert, J. C.; Bjorklund, G. C.; Jundt, D.; Twieg, R. J. *J. Org. Chem.* **1989**, *54*, 3774.
(11) Cha, M.; Neher, D.; Embs, F.; Mittler-Neher, S.; Stegeman, G. I. *Chem. Phys. Lett.* **1993**, *202*, 44.
(12) Kang, C.-S.; Heldmann, C.; Winkelhahn, H.-J.; Schulze, M.; Neher, D.; Wegner, G.; Wortmann, R.; Glania, C.; Krämer, P. *Macromolecules* **1994**, *27*, 6156.
(13) Liptay, W. *Angew. Chemie* **1969**, *6*, 195.
(14) Winkelhahn, H.-J.; Schrader, S.; Neher, D.; Wegner, G. *Macromolecules* **1995**, *28*, 2882.
(15) Pschorn, U.; Spiess, H. W.; Hisgen, B.; Ringsdorf, H. *Makromol. Chem.* **1986**, *187*, 2711.
(16) Leisen, J.; Ohlemacher, A.; Boeffel, C.; Spiess, H. W. *Ber. Bunsenges. Phys. Chem.* **1993**, *93*, 1306.
(17) Servay, Th. K. Ph.D. Thesis, Johannes Gutenberg University, Mainz, 1993.
(18) Falk, U. Ph.D. Thesis, Johannes Gutenberg University, Mainz, 1989.
(19) Servay, Th.K.; Winkelhahn, H.-J.; Kalvoda, L.; Schulze, M.; Böffel, C.; Neher, D.; Wegner, G. *Ber. Bunsenges. Phys. Chem.* **1993**, *97*, 1272.
(20) Hansen, M. T.; Boeffel, C.; Spiess, H. W. *Colloid Polym Sci*, **1993**, *271*, 446.
(21) Winkelhahn, H.-J.; Servay, Th.K.; Kalvoda, L.; Schulze, M.; Neher, D.; Wegner, G. *Ber. Bunsenges. Phys. Chem.* **1993**, *97*, 1287.
(22) Eich, M.; Sen, A.; Looser, H.; Bjorklund, G. C.; Swalen, J. D.; Twieg, R.; Yoon, D. Y. *J. Appl. Phys.* **1989**, *66*, 2559.
(23) Schüssler, S.; Richert, R.; Bässler, H. *Macromolecules*, **1994**, *27*, 4318.
(24) Winkelhahn, H.-J.; Servay, Th.K.; Neher, D. *Ber. Bunsenges. Phys. Chem.* **1996**, *100*, 123.
(25) Ferry, J. D. *J. Am. Chem. Soc.* **1950**, *72*, 3746.
(26) Wegner, G.; Neher, D.; Heldmann, C.; Servay, Th.K.; Winkelhahn, H. J.; Schulze, M.; Kang, C.-S. *MRS Symp. Proc.* **1994**, *328*, 15.
(27) Dhinojwala, A.; Wong, G. K.; Torkelson, J. M. *J. Chem. Phys.* **1994**, *100*, 6046.
(28) Burland, D. M.; Miller, R. D.; Walsh, C. A. *Chem. Rev.* **1994**, *94*, 31.
(29) Mitchell, M. A. *Trends Polym. Sci.* **1993**, *1*, 144.
(30) Köhler, W.; Robello, D. R.; Dao, P. T.; Willand, C. S.; Williams, D. J. *Mol. Cryst. Liq. Cryst. Sci. Technol. B* **1992**, *3*, 83.
(31) Xu, C.; Wu, B.; Becker, M. W.; Dalton, L. R.; Ranon, P. M.; Shi, Y.; Steier, W. H. *Chem. Mater.* **1993**, *5*, 1439.
(32) Wright, M. E.; Mullick, S.; Lackritz, H. S.; Liu, L.-Y. *Macromolecules* **1994**, *27*, 3009.
(33) Block, H.; Shaw, C. P. *Polymer* **1992**, *33*, 2459.
(34) Weder, C.; Neuenschwander, P.; Suter, U. W.; Pêtre, P.; Kaatz, P.; Günter, P. *Macromolecules* **1994**, *27*, 2181.
(35) Weder, C.; Neuenschwander, P.; Suter, U. W.; Pêtre, P.; Kaatz, P.; Günter, P. *Macromolecules* **1995**, *28*, 2377.

MA960353B